NiO-ZnO Nanoheterojunction Networks for Room-Temperature Volatile Organic Compounds Sensing

Hongjun Chen[1], Renheng Bo[1], Aabhash Shrestha[1], Bobo Xin[1], Noushin Nasiri[1,2], Jin Zhou[1], Iolanda Di Bernardo[1], Aaron Dodd[3], Martin Saunders[3], Josh Lipton-Duffin[4], Thomas White[5], Takuya Tsuzuki[6] and Antonio Tricoli[1]**

[1]Nanotechnology Research Laboratory, Research School of Engineering, College of Engineering and Computer Sciences, Australian National University, Canberra 2601, Australia.

[2]Institute for Biomedical Materials and Devices, Faculty of Science, University of Technology Sydney, Sydney, NSW 2007, Australia

[3]Centre for Microscopy Characterisation and Analysis, the University of Western Australia (M010), 35 Stirling Highway, Perth, WA 6009, Australia

[4]Institute for Future Environments (IFE) and Central Analytical Research Facility (CARF), Queensland University of Technology (QUT), Brisbane, QLD 4000, Australia

[5]Research School of Engineering, College of Engineering and Computer Sciences, Australian National University, Canberra 2601, Australia.

[6]Laboratory of Advanced Nanomaterials for Sustainability, Research School of Engineering, College of Engineering and Computer Sciences, Australian National University, Canberra 2601, Australia.

Keywords: *chemical sensors; nanoheterojunctions; room-temperature; flame synthesis; volatile organic compounds*

**Corresponding authors: antonio.tricoli@anu.edu.au; hongjun.chen@anu.edu.au;*

Abstract

Engineering of highly performing nanomaterials, capable of rapid detection of trace concentrations of gas molecules at room temperature, is key to the development of the next generation of miniaturized chemical sensors with application extending from personalized medical diagnostics to public space safety and environmental monitoring. Here, we present a highly performing nanoheterojunctions layout for the rapid room-temperature chemical sensing of volatile organic compounds down to 10 particles per billion concentrations. The layout consists of a three-dimensional network of NiO-ZnO p-n semiconductors with grain size of ca. 20 nm nanometres and a porosity of ca. 98%. Notably, we observe that the formation of the p-n heterojunctions by decoration of a ZnO nanoparticle networks with NiO increases the sensor response by more than 4 times, while improving the lower limit of detection. Under solar light irradiation, the optimal NiO-ZnO nanoheterojunction networks demonstrate a strong and selective room-temperature response to two important volatile organic compounds utilized for breath analysis, namely acetone and ethanol. Furthermore, these NiO-ZnO nanoheterojunctions show an inverse response to acetone from that observed for all others reducing gas molecules (i.e. ethanol, propane and ethylbenzene) responding with an increase and decrease of their resistivity to the former and the latter, respectively. We believe that these novel insights of the optoelectrochemical properties of ultraporous nanoheterojunctions networks provide guidelines for the future design of low-power solid-state chemical sensors that can be integrated in wearable and portable devices for numerous emerging applications including detection of volatile biomarkers and explosives.

Introduction

Sensing of ultra-low concentrations of volatile organic compounds (VOCs) is becoming increasingly important, due to their potential as non-invasive biomarkers for medical diagnostics.[1] Notably, several VOCs present in the human breath are related to the important metabolic processes and can serve as an effective non-invasive tool for health monitoring.[1, 2] For instance, abnormal concentrations of ethanol and acetone in the breath have been recognised as biomarkers for diseases such as non-alcoholic fatty liver disease, hepatic steatosis and diabetes.[3] Despite the potential of human breath analysis for the early-stage diagnosis and monitoring of several diseases by point-of-care or wearable devices, its future implementation requires the development of highly sensitive chemical gas sensors capable of selectively measuring ppb to ppt concentrations of VOCs in complex gas mixtures such as the human breath with possibly low-power consumption.[1-4]

Metal oxide semiconductor (MOS)-based chemical sensors can fulfil many of the requirements for breath analysis, due to their high sensitivity, ease of miniaturisation and low cost.[5] However, MOS sensors are typically operated at relatively high temperatures of 200 - 400 C,[5-8] which not only increases the power consumption but also the complexity of the sensors layout and overall device. Furthermore, the high temperature operation induces crystal growth of metal oxides resulting in a reduced long-term stability.[5, 9] Recently, various nanostructured designs such as one-dimensional (1D) metal oxide nanostructures, noble metal doping/modification, and light-activated nanomaterials have been explored to decrease the operation temperature of MOS sensors while trying to preserve their excellent lower limit of detection in the ppb range.[9-12]

Many different MOS such as ZnO, SnO_2, TiO_2 and In_2O_3 have been investigated for light-powered gas sensing at low temperature.[13-20] In particular, nanostructured MOS have demonstrated significant potential for gas sensing owing to their large surface-to-volume

ratio, high specific surface area, and abundant reactive surface sites.[5,9-11,21,22] Different MOS nanostructures such as Bi_2O_3-core/ZnO-shell nanobelt, SnO_2 functionalized GaN nanowire, SnO_2-core/ZnO-shell nanowires, ZnO nanorods and fibers have been utilised to enhance the material low temperature gas sensing performance.[10,11,13,23-26] Despite significant progress, the sensitivity and detection limits of MOS gas sensors are in the range of ppm level and required further improvements for many applications including their use in breath analysis devices.

Use of heterojunctions of the metal oxide semiconductors is a promising approach to improve the light-assisted gas sensing performance of MOS sensors.[12,27] An effective interface between the heterojunction can provide intimate electrical contact between different semiconductors and improve interfacial charge transfer.[12] Especially, p-n heterojunction between the semiconductors are interesting due to the formation of a charge depletion layer at their interface.[12] Flame synthesis is a scalable method for the synthesis of metal oxide nanoparticles and films with controlled primary nanoparticle sizes and structural properties.[5] In particular, it allows the *in situ* fabrication of highly porous semiconductor nanoparticle networks[28] with primary particle size below two times of Debye length.[6] Flame synthesis of various nanostructured films has been previously reported for applications as VOC sensors such as Si doped WO_3,[13,14] Si doped SnO_2,[15] and CuO dispersed SnO_2[16] demonstrating limit of detection of few ppb. However, these systems generally require elevated operating temperatures and such highly resistive ultraporous nanoparticle networks have not been able to be utilized at room temperature.

Here, we report the fabrication of novel ultraporous p-n heterojunction networks comprising of n-type zinc oxide (ZnO) nanostructures and p-type nickel oxide (NiO) for enhanced VOC gas sensing at room temperature. The ultraporous ZnO nanostructures were fabricated by flame synthesis and aerosol self-assembly of nanoparticle networks. Thereafter, NiO was

sputtered on the ZnO nanostructures to create an ultraporous NiO-ZnO p-n nanoheterojunction, which was utilized to sense important VOCs such as ethanol, acetone, propane and ethylbenzene. Under solar light illumination, these NiO-ZnO gas sensor devices demonstrate excellent room-temperature sensitivity to two common medical VOCs detecting acetone and ethanol gas (~10 ppb). The impact of simultaneous light irradiation and thermal activation was explored demonstrating to extend the detection limit down to 2 ppb at an optimal operating temperature of 150 ^{o}C. Moreover, an excellent selectivity to acetone was observed at room temperature, which can be utilised to develop portable and point-of-care devices for the diagnostics of type 1 diabetes.

Results and discussion

A schematic description of the chemical sensor layout is shown in **Figure 1**a. An ultraporous ZnO film is deposited on interdigitated Pt electrodes by thermophoretic deposition of flame-made ZnO nanoparticle aerosols.[28] The thickness of ZnO film can be controlled linearly by increasing the aerosol deposition times.[5, 28] A thickness of ~6 μm of ZnO has been selected in line with previous literature on high performance visible-blind UV-photodetectors.[28] This results in a porosity of 98% and a bi-modal hierarchical pore size distribution with large pores of 1-4 mm and small mesopores of few tens of nms (**Fig. S1**a-c). Subsequently, a NiO bulk thickness from 1 to 9 nm was sputtered on these ultraporous films increasing the sputtering deposition time from 5 to 45 s to form NiO-ZnO heterojunction networks with controlled NiO content. These NiO-ZnO films were further annealed at 300 °C for 12 hours to improve the interparticle connectivity and carrier transport through the grain boundaries. Light illumination induces the formation of photo-generated electron-hole, in the semiconductors, which are efficiently separated by the p-n nanoheterojunctions formed by at the NiO-ZnO interface. The generated electrons are trapped on the surface resulting in the formation of highly reactive photo-induced oxygen ions. The introduced VOC molecules are

then oxidized by these oxygen ions releasing the trapped electrons and increasing the NiO-ZnO film conductivity. The resulting change in film resistance, or rise in photocurrent, can be utilized for sensing numerous VOCs.

Figure 1b,c and **Figure S1**d,e show scanning electron microscopy (SEM) images of as deposited 9 nm NiO on ZnO films after annealing at 300 ^{o}C. For comparison, SEM images of the pure ZnO film are also shown in **Figure S1**a-c. The SEM analysis reveals that upon NiO sputtering the films retain the typical fractal-like morphology with micron-sized pores between partially sintered nanoparticles, which is obtained by aerosol deposition of nanoparticles in the diffusion regime.[6,14,23,6,28] Similarly, the cross-sectional SEM images (**Figure 1**c) of the films show no visible cracks nor other defects in line with previous reports.[5,6,8,28] The penetration of the NiO in the ZnO nanoparticle network was recently validated for similar NiO-ZnO nanoheterojunctions used for UV-photodetectors.[29] **Figure 2**a shows a transmission electron microscopy (TEM) of NiO coated ZnO particles that were collected from the films made with a sputtering time of 1 nm of NiO. The TEM images shows that the NiO-ZnO nanoparticles are quasi-spherical in shape with primary particles of ca. 20 nm agglomerated in larger fractal structures (**Figure 2**a). Furthermore, their high-resolution TEM (HRTEM) images reveal the crystalline features of ZnO with a lattice spacing of ca. 0.26 nm (**Figure 2**b), which is consistent with the (002) plane of ZnO.[30] The selected area electron diffraction (SAED) patterns of these particles also verify the crystallinity of ZnO (**Figure 2**a, inset). It is noted that the diffraction rings of NiO could not be discerned for any samples due to the low mass fraction of NiO. In order to further investigate the formation of NiO-ZnO nanoheterojunctions as a function of the NiO content, the 9 nm NiO-ZnO nanostructures were investigated by TEM (**Figure** S2). It was observed that at a NiO average thickness of 9 nm, the originally smooth surface of the ZnO nanoparticles (**Figure** S2b) becomes very rough indicating the formation of a series of

nanoheterojunctions. The X-ray diffraction (XRD) spectra of the 9 nm NiO-ZnO films further confirm the high crystallinity of ZnO (**Figure 3**a) with an hexagonal wurtzite structure (JCPDS No. 36-1451).[28] In line with the SAED, it was not possible to detect the NiO XRD patterns, due to the low mass content of the latter.

To ascertain the presence of the NiO, energy-dispersive X-ray spectra (EDS) were obtained from the NiO-ZnO films (**Figure** 3c). The EDS spectra of the 9 nm NiO-ZnO film shows the presence of both the Ni and Zn peaks, while no Ni peaks can be observed on the pure ZnO films. High angle annular dark field images of the NiO-ZnO particles and their corresponding element mapping further confirm the successful deposition of NiO on the ZnO surface (**Figure 2**c and d). It is observed that Zn, Ni and O are uniformly distributed on the surface of 1 nm NiO-ZnO particles. Similarly, Fourier Transform Infrared (FTIR) spectra were used to verify the composition of NiO-ZnO films (**Figure 3**b). FTIR spectra shows that the ZnO peaks at 505 and 430 cm^{-1} disappears and a new peak at 521 cm^{-1} is formed after sputtering of NiO, which is ascribed to the presence of Ni–O stretching vibration.[33] Furthermore, the FTIR peaks at 3450, 1134 and 900 cm^{-1} suggest the adsorption of atmospheric moisture and are assigned to the O–H stretching and bending vibrations of the hydroxyl groups.[28] The peaks at 1600 and 1400 cm^{-1} can be attributed to the asymmetrical and symmetrical stretching of carboxylate groups.[28] **Figure 3**d shows the optical absorption spectra of the NiO-ZnO films as a function of the NiO thickness. We see that the NiO-ZnO films have a prominent cut-off absorption located at ca. 375 nm, corresponding to the band gap of ZnO. No shift in the optical absorption spectra of ZnO can be observed upon deposition of NiO. This indicates that NiO does not alter the optical properties of ZnO as expected from its higher bandgap of 3.6 eV vs the 3.2 eV of the ZnO. X-ray photoelectron spectroscopy (XPS) was conducted on the pure ZnO and 1 nm NiO-ZnO nanoheterojunction films. Figure 3e,f show the high-resolution XPS spectra of the Zn 2p and Ni 2p. The binding energy of Zn 2p is not shifted by

the deposition of NiO (**Figure** 3e), while the Ni 2p signal is only detected for the 1 nm NiO-ZnO films (**Figure** 3f). These spectra further validate the successful formation of a NiO-ZnO nanoheterojunction structure.

To investigate the potential of these flame-made ultraporous NiO-ZnO nanoheterojunctions for room-temperature chemical sensing, ethanol was initially chosen as a model analyte, due to its common use for testing of MOS devices. As shown in **Figure 1**a, the response of the NiO-ZnO gas sensors was recorded by monitoring the current change under a constant applied voltage. **Figure S3** shows the dynamic response of pure ZnO film at room temperature when dosed with the different concentrations of ethanol gas in dark and under light illumination (AM1.5 solar simulator, 67 $mWcm^{-2}$). In line with previous report, the pure ZnO films had no detectable response to the ethanol in dark condition.[18,34,35] Notably, the sensor response, defined as $(I_{analyte}/I_{air})$ -1, increases significantly under light irradiation and this effect is rapidly lost once the light source is switched off. The sensor response increases from 0.2 to 0.62 with increasing ethanol concentration from 0.2 to 1 ppm indicating that even the pure ZnO nanoparticle networks can be utilized for ethanol sensing at room temperature under light irradiation.

Notably, deposition of NiO on the ZnO strongly enhanced the sensor response to ethanol. The sensor response of ZnO films to 1 ppm of ethanol increased from 0.62 to 2.6 after deposition of 1 nm NiO (**Figure 4**a) and the detection limit reached as low as 10 ppb (**Figure S4**). Varying the NiO thickness and the sensor operating temperature influenced the sensor response and sensitivity. **Figure 4**b compares the room temperature sensor response at different concentrations of ethanol as a function the NiO thickness. The 1 nm NiO-ZnO showed the highest enhancement in sensor response and sensitivity. Increasing the NiO bulk thickness from 1 to 5 nm decreased the sensor response, which, however, remained comparable when further increasing the NiO thickness to 9 nm. Nevertheless, all the NiO-

ZnO nanoheterojunctions demonstrated a higher sensor response than that of the pure ZnO sensors (e.g. 1.66 at 1 ppm ethanol for the 5 nm NiO vs. 0.62 for the pure ZnO). **Table 1** shows a comparative summary of the NiO-ZnO performance with other literature on light-assisted chemical sensors operating at room temperature.[17,22,26,34,36-40] Notably, the 1 nm NiO-ZnO film exhibits significantly higher sensitivity (between 3-60 times higher at 1 ppm of ethanol) and ca. 2000 times lower limit of detection than several other recent studies.[13, 20,22,26,34,36-40]

Further insights on the performance and sensing mechanism of the NiO-ZnO were obtained through investigating the correlation between sensitivity and responsivity. **Figure 4**c shows the sensor response of the 1 nm NiO-ZnO films at different operation temperatures. It was observed that the sensor response increases with increasing operation temperature from 30 to 150 °C achieving a record-high response of ~29 to 1 ppm of ethanol. This is a ca. 11 times enhancement as compared to its response of ~2.6 at room temperature (**Figure 4**a). However, further increasing the operation temperature to 250 and 300 °C decreased the sensor response to ethanol, with exception of that to 1 ppm of ethanol at 250 °C. This is attributed to the increased catalytic activity of these films with increasing operating temperature that combust most of the ethanol molecules before reaching the most sensitive bottom layer of the device in proximity of the interdigitated electrodes.[8] Furthermore, an operation temperature of 150 ^{o}C with light illumination enables to achieve an excellent sensitivity with a detection limit down to 2 ppb ethanol (**Figure** 4d). Notably, this is the highest sensitivity so far reported for light-assisted ethanol chemical sensors (see **Table 1**) made of single semiconductors and p-n heterojunctions (see **Table 2**).[17,22,36-38]

The selectivity of the NiO-ZnO nanoheterojunctions to different VOCs was further evaluated with acetone, ethylbenzene and propane. It was observed that the NiO-ZnO films have an excellent selectivity for ethanol over the latter two VOCs (**Figure 4**e) with a sensor response

to ethanol of ~15 times higher than that for ethylbenzene and propane. Interestingly, the sensor response to acetone was reversed showing a drop of the measured current, a phenomenon that is normally demonstrated by p-type semiconductors.[27] To further elucidate this acetone sensor response, the sensor response to 1 ppm of acetone was investigated as a function of the temperature. It was observed that the sensor resistance decreases gradually while the sensor response to acetone gas switched from a negative to a positive value as the operation temperature was increased from 30 to 150 ^{o}C (**Figure 4**f). Notably, the transition point for the sensor response occurred between 100 - 120 ^{o}C (**Figure S5**). This suggests that the negative response might be due to the interaction of the moisture adsorbed on the nanostructured surface with the acetone molecules, and it is lost once the surface temperature is above the water condensation point. Importantly, this negative response to acetone at room temperature can be utilized to selective sense this important analyte for breath analysis. In fact, the NiO-ZnO films show excellent response to acetone at different concentrations at room temperature and can be utilized for the selective detection of acetone gas at ambient conditions (**Figure S6**).

The excellent performance of these NiO-ZnO films as gas sensors is attributed to (a) the formation of p-n heterojunctions between NiO and ZnO, which can enhance the separation of the photogenerated electron-hole pairs, and (b) the unique ultraporous morphology of the NiO-ZnO films with electron-depleted NiO and ZnO domains (i.e. less than Debye length). A possible mechanism is suggested below, under ambient conditions, the nanostructured NiO-ZnO adsorbs O_2 on its surface, which results in the trapping of electrons from the semiconductors conduction bands to form the oxygen ion (O_2^-) in dark condition.[31] Usually, these oxygen ions are thermally stable at low temperature and cannot desorb from the NiO-ZnO surface.[31] Thus, the NiO-ZnO film shows no response for gas sensing in dark condition (see **Figure 4**a).[18,38] Upon illumination, photon absorption occurs within ZnO layer (as NiO

does not contribute significantly to the optical absorbance, see **Figure 3**d) and the photogenerated charge carriers can be separated at the NiO-ZnO interface due to Fermi level mediated charge transfer between NiO and ZnO (**Figure S7**).[29] This significantly reduces the possibility of electron-hole recombination and increases the density of photogenerated electrons (**Figure S8**). These photo-generated electrons can react with the ambient oxygen molecules to form photo-induced oxygen ions ($O_2 + e^- (h\nu) \rightarrow O_2^- (h\nu)$), that have high reactivity in comparison to the chemisorbed oxygen ions (O_2^-).[18,38] When the sensor is exposed to a reducing gas such as ethanol under solar irradiation, these photo-induced oxygen ions will participate in the redox reactions at room temperature (e.g. $C_2H_5OH + 3O_2^- (h\nu) \rightarrow 2CO_2 + 3H_2O + 3e^-$) and release electrons in the process.[31] This increases the conductivity of the NiO-ZnO films and leads to an increase in the measured current (**Figure 4**a). We propose that the formation of highly active photo-induced oxygen ions is the main contributor to the enhancement of the NiO-ZnO sensor performance at low temperatures. The formation of NiO-ZnO nanoheterojunctions improve the separation of photo-generated electron/hole pairs increasing the formation of photo-induced oxygen ions, and thus the concentration of highly reactive surface sites for chemical sensing. As a result, while both the pure ZnO and the NiO-ZnO are activated by light illumination, the p-n nanoheterojunction sensors have a significantly improved chemoresistive sensor response. In addition, the hierarchical ultraporous nanostructure morphology of the NiO-ZnO nanoheterojunctions facilitates the penetration of gases into the film layers allowing to a larger fraction of the film to participate in the gas sensing process.[28] Meanwhile, the high surface area of the ultraporous nanostructure also provide a large amount of active sites for the gas sensing,[28] which enhances sensor sensitivity and decreases the lower limit of detection significantly over that previously reported.

Conclusions

A novel ultraporous NiO-ZnO nanoheterojunction layout was demonstrated for the room-temperature sensing of volatile organic compounds. Chemical sensing devices were rapidly fabricated by aerosol deposition of an ultraporous network of flame-made nanoparticles and their NiO decoration by sputtering. An enhancement of ~4-5 times in the sensor response at room temperature was observed after NiO deposition when compared to the pure ZnO films achieving a record-low detection limit of 10 ppb ethanol. The NiO-ZnO sensor mechanism and performance was further investigated as a function of the sensor operation temperature. The room temperature sensor response was enhanced by ca. 10 folds when operated at an optimal working temperature of 150 ^{o}C reaching a detection limit of 2 ppb ethanol. Notably, an excellent dual selectivity to ethanol and acetone was observed with the acetone inducing an opposite negative response at room temperature than that to ethanol. The enhanced sensing performance of these NiO-ZnO nanostructures is ascribed to its unique ultraporous morphology and the formation p-n nanoheterojunctions, which promote the separation of the photo-generated electron-holes and their interaction with the target analyte molecules. We believe that this highly performing nanostructured layout and insight can provide guidance for the design of the next generation of miniaturized chemical sensors for portable and point-of-care monitoring and sensing of volatile biomarkers.

Experimental section

A flame spray pyrolysis (FSP) system was used for the synthesis and direct deposition of ZnO nanoparticles films onto Pt interdigitated electrodes. The ultraporous ZnO and NiO-ZnO films were prepared as follows: A total Zn-metal atom concentration of 0.3 mol L^{-1} was prepared by diluting zinc naphthenate (10% Zn, Sigma–Aldrich) in xylene (Sigma–Aldrich). This solution was supplied through a syringe pump at a rate of 5 mL min^{-1}, and dispersed into a fine spray with 7 L min^{-1} oxygen at a constant pressure drop of 2 bars. The spray was ignited by supporting premixed methane/oxygen flames (CH_4 = 1.2 L min^{-1}, O_2 = 2 L min^{-1}).

A water-cooled substrate holder placed at 20 cm height above the burner (HAB) was utilized to keep the substrate temperature below 150 °C. NiO was deposited by an AJA ATC 2400 magnetron sputtering system using a Ni target in an Ar/O_2 ambient (18/2 sccm). The chamber was evacuated to 9×10^{-7} Torr before deposition and sputtering deposition was performed at a gas pressure of 4×10^{-3} Torr for 5, 25 and 45 seconds at room temperature with a power of 200 W. The gas sensor substrate was made of glass with interdigitated Pt lines with 5 μm width and spacing and a total electrode area of 7 mm × 5 mm (G-IDEAU5, DropSens, Oviedo, Spain). All substrates were cleaned 3 times by ethanol before FSP deposition. The substrates were kept in a furnace (Brother High Temperature Furnace XD-1.2KN) at 300 °C for 12 h at ambient pressure prior measurement, to stabilize the nanoparticle size and avoid resistive-sintering during the gas sensing measurements.

High Angle Annular Dark Field Scanning Transmission Electron Microscopy (HAADF-STEM) imaging and element mapping were carried out using a FEI Titan G2 80-200 TEM/STEM with ChemiSTEM Technology operating at 200 kV. The elemental mapping was obtained by energy dispersive X-ray spectroscopy using the Super-X detector on the Titan with a probe size ~1 nm and a probe current of ~0.4 nA. The morphology and its EDS analysis were investigated by a Hitachi H7100FA TEM at 100 kV and an analytical SEM, using Zeiss Ultraplus (FESEM) at 3 kV. The surface compositions were analyzed by Fourier transform infrared spectroscopy (FTIR-ATR, Bruker-Alpha, U.S.A). The crystalinity was characterized by X-ray diffraction using Bruker system (XRD, D 2 Phaser, USA) equipped with Cu Kα radiation of average wavelength 1.54059 Å. The absorbance spectra were measured with a Perkin–Elmer (Lambda 1050 UV/vis/NIR) Spectrophotometer and a 150 mm integrating sphere. X-ray photoelectron spectroscopy (XPS) spectra were collected in a Thermofisher Kratos Axis Supra photoelectron spectrometer, with a monochromated Al k_α source (1486.7 eV) at pass energy 20.

The sensor measurements were performed as follow: VOCs (ethanol, 9.91 ppm in N_2, Coregas; acetone, 10.1 ppm in N_2, Coregas; ETBZ, 10 ppm in N_2, BOC gas; and PROP, 10 ppm in N_2, BOC gas) was controlled by a mass flow controller (Bronkhorst) and further diluted with simulated air (0.1 L/min O_2 + 0.4 L/min N_2, BOC) to reach the desired concentration (from 2 ppb to 1 ppm) and the total gas flow rate was still kept at 0.5 L/min. The temperature of the hotplate in a chamber (Linkam) was controlled by a temperature controller and the sample was illuminated through a quartz window by a solar simulator (NewSpec, LCS-100) with an AM1.5 filter glass. The dynamic response of gas sensor was recorded by an electrochemical workstation (CHI 660E, USA) at a constant applied voltage of 1 V.

Acknowledgements

R.B., N.N., A.D., M.S., I.D.B., J.L.D. and H.C. performed materials synthesis, characterization and gas sensing measurements. H.C., N.N. T.T. and A.T. contributed to the data analysis and writing of the manuscript. A.T. gratefully acknowledges the support of Australian Research Council DP150101939, Australian Research Council DE160100569, and Westpac 2016 Research Fellowship. The XPS analyses were conducted in CARF (Central Analytical Research Facility) of the Queensland University of Technology.

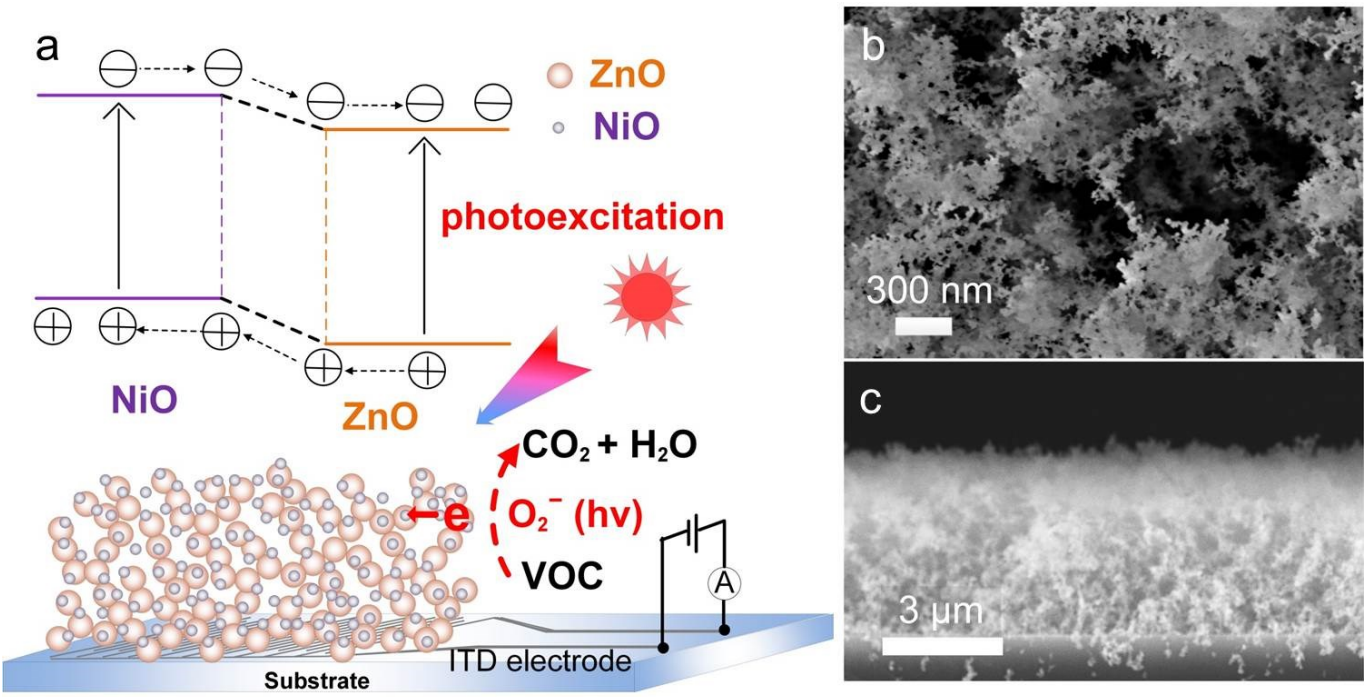

Figure 1. Schematic of the p-n NiO-ZnO nanoheterojunctions devices for chemoresistive sensing of VOC (a). SEM images of exemplary films with a NiO and ZnO thickness of 9 nm NiO and 6 µm ZnO, respectively. A highly porous and uniform (b) surface and (c) cross-sectional morphology is observed.

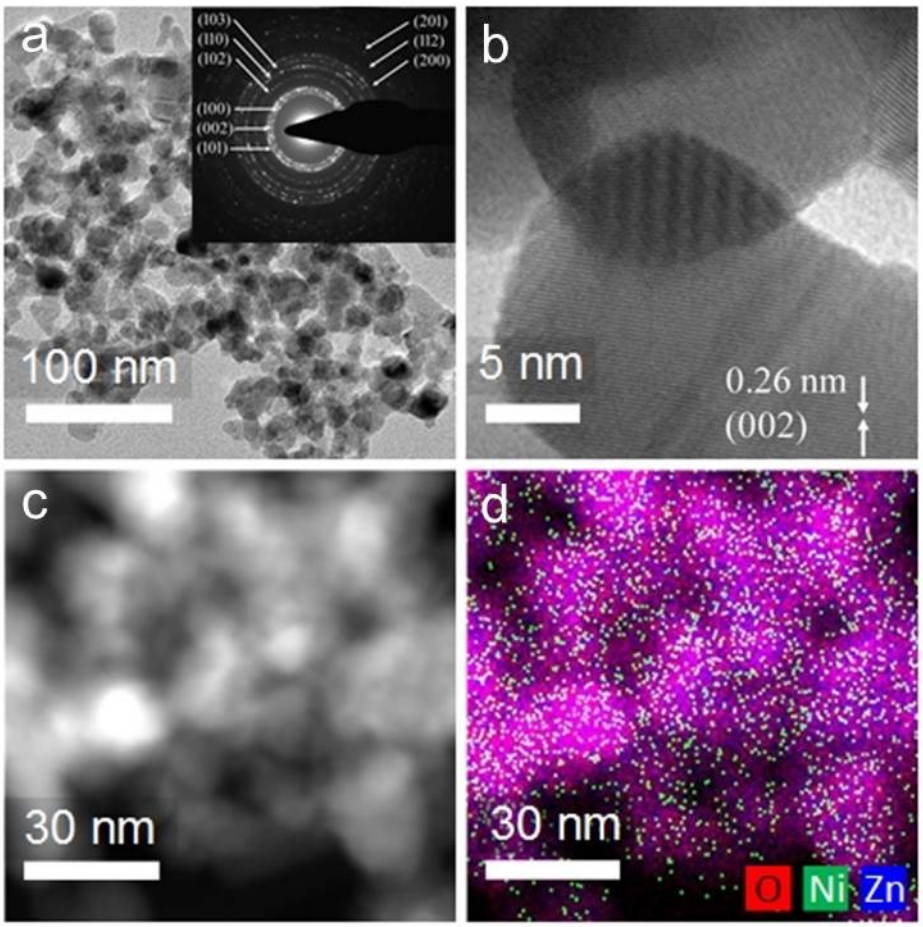

Figure 2. TEM (a), HRTEM (b), high angle annular dark field (c) and elemental image mapping of 1nm NiO-ZnO (d), inset in (a) is its SAED pattern.

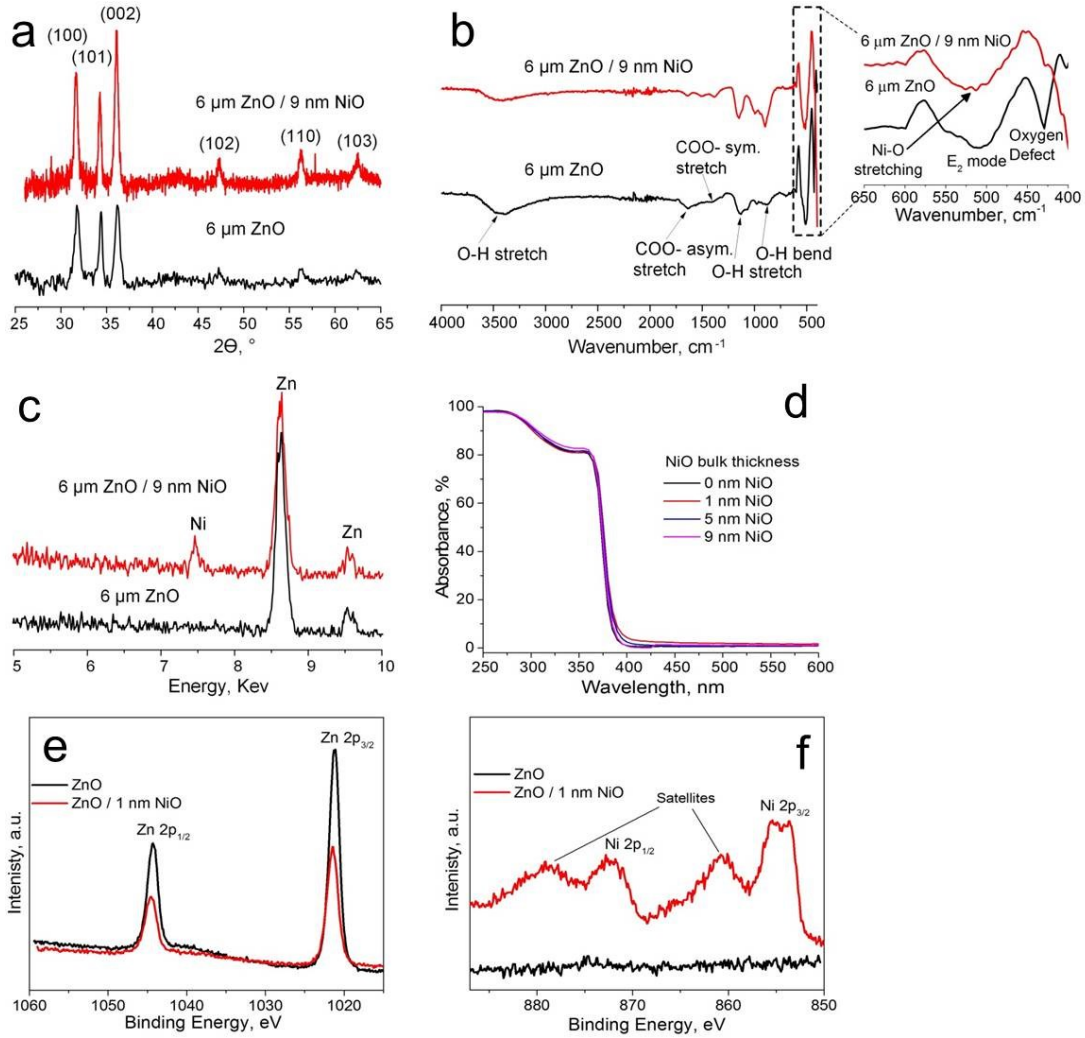

Figure 3. XRD (a), FTIR (b), and EDS (c) spectra of the pure ZnO and 9 nm NiO-ZnO and the absorbance spectra of the pure ZnO as a function of the NiO bulk thicknesses (d), and high-resolution XPS spectra of the Zn 2p (e) and Ni 2p (f) for the pure ZnO and 1 nm NiO-ZnO

nanoheterojunction films.

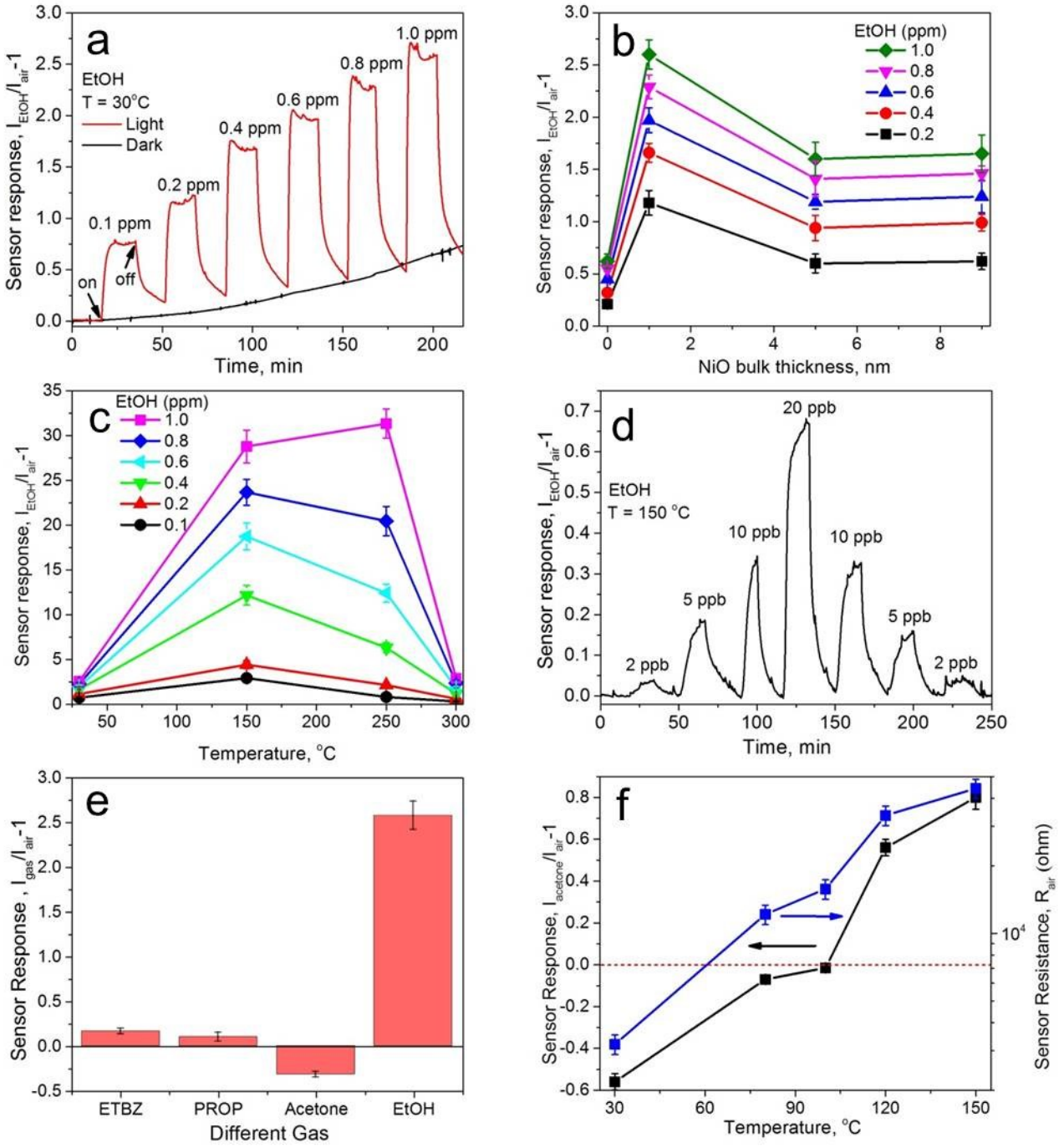

Figure 4. Dynamic responses of 1 nm NiO-6 µm ZnO nanoheterojunction film to ethanol molecules as a function of its concentration from 0.1 to 1 ppm at room temperature in dark or under solar irradiation (a). Ethanol response of 6 µm ZnO nanoparticle films as a function of the NiO thickness at room temperature under solar irradiation (b). Response of a 1 nm NiO-ZnO nanoheterojunction film as a function of temperature and ethanol concentration from 0.1 to 1 ppm under solar irradiation (c). Dynamic responses of a 1 nm NiO-ZnO film to ethanol

with concentrations from 2 to 20 ppb at 150°C under solar irradiation (d). Sensor response of a 1 nm NiO-ZnO film to 1 ppm of ethylbenzene, propane, acetone and ethanol at 30°C under solar irradiation (e). Sensor responses and resistance of a 1 nm NiO-ZnO film to 1 ppm of acetone as a function of the temperature (f).

Table 1. Comparison of light-assisted VOC gas sensing at room temperature.

Material	Temperature	Responsivity (I_{EtOH}/I_{air}-1) to EtOH (ppm)	LOD* (ppm)	Ref.
ZnO-NiO nanoheterojunction	RT*	0.77 (0.1) 2.6 (1.0)	0.01	This work
ZnO nanoparticles	RT	0.3 (100) 1.2 (800)	N/A	31
ZnO fibers	RT	0.04 (10) 0.8 (60)	N/A	13
ZnO nanodisks	RT	0.17 (100) 0.73 (500)	20	32
ZnO nanorods	RT	1.26 (220)	N/A	33
Cu-doped ZnO nanocrystals	RT	0.37 (1120)	N/A	34
Au decorated ZnO nanofibers	RT	0.53 (20)	N/A	35
hollow TiO_2 microspheres	RT	0.8 (3.0)	N/A	18
SnO_2 functionalized GaN nanowire	RT	1.55 (500)	N/A	24

LOD*, limit of detection; RT*, room temperature

Table 2. Comparison of p-n heterojunction nanostructures for VOC sensing.

Material	Temperature (°C)	Responsivity (I_{EtOH}/I_{air}-1) to EtOH (ppm)	LOD$^+$ (ppm)	Ref.
ZnO-NiO nanoheterojunctions	150	1.95 (0.1) 29 (1.0)	0.002	This work
CuO decorated SnO_2 nanoparticles	320	0.5 (0.02) 50 (10)	N/A	8
Mn_3O_4-decorated ZnO nanobelts	400	ca. 6 (2.5)$^{\#}$	0.15*	36
Bi_2O_3-decorated In_2O_3 nanorods	200	ca. 1 (10)$^{\#}$ 16.74 (200)	N/A	37
TiO_2 modified Co_3O_4 nanowire	160	ca. 20 (10)$^{\#}$	N/A	38
NiO-functionalized SnO_2 hollow spheres	450	0.75 (20)	N/A	39
nano-coaxial p-Co_3O_4/n-TiO_2 heterojunction	260	39 (100)	N/A	40
NiO-decorated ZnO nanowire	450	0.82 (0.05) 25.15 (5.0)	0.017*	41
Co_3O_4-decorated ZnO nanowire	400	Ca. 6 (5.0)	0.47*	42

LOD$^+$, limit of detection; $^{\#}$ extracted from the figures; * calculated based on $R_{air}/R_{gas} \geq 1.2$

References

1. A. Tricoli, N. Nasiri and S. De, *Adv. Funct. Mater.*, 2017, **27**, 1605271.
2. I.-D. Kim, S.-J. Choi, S.-J. Kim and J.-S. Jang, in *Smart Sensors for Health and Environment Monitoring*, ed. C.-M. Kyung, Springer Netherlands, Dordrecht, 2015, 19-49.
3. T. Ulrike and H. Hossam, *J. Breath Res.*, 2014, **8**, 027103.
4. S. F. Solga, A. Alkhuraishe, K. Cope, A. Tabesh, J. M. Clark, M. Torbenson, P. Schwartz, T. Magnuson, A. M. Diehl and T. H. Risby, *Biomark.*, 2006, **11**, 174-183.
5. A. Tricoli, M. Righettoni and A. Teleki, *Angew. Chem. Int. Ed.*, 2010, **49**, 7632-7659.
6. A. Tricoli, M. Graf, F. Mayer, S. Kuühne, A. Hierlemann and S. E. Pratsinis, *Adv. Mater.*, 2008, **20**, 3005-3010.
7. A. Tricoli, M. Graf and S. E. Pratsinis, *Adv. Funct. Mater.*, 2008, **18**, 1969-1976.
8. A. Tricoli and S. E. Pratsinis, *Nat Nano*, 2010, **5**, 54-60.
9. J. Zhang, X. Liu, G. Neri and N. Pinna, *Adv. Mater.*, 2016, **28**, 795-831.
10. K. J. Choi and H. W. Jang, *Sensors*, 2010, **10**, 4083.
11. M. M. Arafat, B. Dinan, S. A. Akbar and A. S. M. A. Haseeb, *Sensors*, 2012, **12**, 7207.
12. D. R. Miller, S. A. Akbar and P. A. Morris, *Sens. Actuators B*, 2014, **204**, 250-272.
13. J. Gong, Y. Li, X. Chai, Z. Hu and Y. Deng, *J. Phys. Chem. C*, 2010, **114**, 1293-1298.
14. S.-W. Fan, A. K. Srivastava and V. P. Dravid, *Appl. Phys. Lett.*, 2009, **95**, 142106.
15. M. Law, H. Kind, B. Messer, F. Kim and P. Yang, *Angew. Chem. Int. Ed.*, 2002, **41**, 2405-2408.
16. E. Comini, G. Faglia and G. Sberveglieri, *Sens. Actuators B*, 2001, **78**, 73-77.
17. D. Haridas, A. Chowdhuri, K. Sreenivas and V. Gupta, *Sens. Actuators B*, 2011, **153**, 152-157.
18. X. Li, X. Li, J. Wang and S. Lin, *Sens. Actuators B*, 2015, **219**, 158-163.
19. E. Zampetti, A. Macagnano and A. Bearzotti, *J Nanopart Res*, 2013, **15**, 1-8.
20. E. Comini, A. Cristalli, G. Faglia and G. Sberveglieri, *Sens. Actuators B*, 2000, **65**, 260-263.
21. J.-H. Lee, *Sens. Actuators B* 2009, **140**, 319-336.
22. G. Shen, P.-C. Chen, K. Ryu and C. Zhou, *J. Mater. Chem.*, 2009, **19**, 828-839.
23. S. Park, H. Ko, S. Lee, H. Kim and C. Lee, *Thin Solid Films*, 2014, **570,** 298-302.
24. R. Bajpai, A. Motayed, A. V. Davydov, V. P. Oleshko, G. S. Aluri, K. A. Bertness, M. V. Rao and M. E. Zaghloul, *Sens. Actuators B*, 2012, **171–172**, 499-507.
25. S. Park, S. An, Y. Mun and C. Lee, *ACS Appl. Mater. Interfaces*, 2013, **5**, 4285-4292.
26. G. Lu, J. Xu, J. Sun, Y. Yu, Y. Zhang and F. Liu, *Sens. Actuators B*, 2012, **162**, 82-88.
27. H.-J. Kim and J.-H. Lee, *Sens. Actuators B*, 2014, **192**, 607-627.
28. N. Nasiri, R. Bo, F. Wang, L. Fu and A. Tricoli, *Adv. Mater.*, 2015, **27**, 4336-4343.
29. N. Nasiri, R. Bo, L. Fu and A. Tricoli, *Nanoscale*, 2017, **9**, 2059-2067.
30. G. A. Velázquez-Nevárez, J. R. Vargas-García, J. Aguilar-Hernández, O. E. Vega-Becerra, F. Chen, Q. Shen and L. Zhang, *Materials Research*, 2016, **19**, 113-117.
31. Z. Q. Zheng, J. D. Yao, B. Wang and G. W. Yang, *Sci. Rep.*, 2015, **5**, 11070.
32. M. R. Alenezi, A. S. Alshammari, K. D. G. I. Jayawardena, M. J. Beliatis, S. J. Henley and S. R. P. Silva, *J. Phys. Chem. C*, 2013, **117**, 17850-17858.
33. L. Peng, Q. Zhao, D. Wang, J. Zhai, P. Wang, S. Pang and T. Xie, *Sens. Actuators B*, 2009, **136**, 80-85.
34. L. Peng, T.-F. Xie, M. Yang, P. Wang, D. Xu, S. Pang and D.-J. Wang, *Sens. Actuators B*, 2008, **131**, 660-664.

35. Y. Li, J. Gong, G. He and Y. Deng, *Mater. Chem. Phys.*, 2012, **134**, 1172-1178.
36. C. W. Na, S.-Y. Park, J.-H. Chung and J.-H. Lee, *ACS Appl. Mater. Interfaces*, 2012, **4**, 6565-6572.
37. S. Park, S. Kim, G.-J. Sun and C. Lee, *ACS Appl. Mater. Interfaces*, 2015, **7**, 8138-8146.
38. L. Zhang, Z. Gao, C. Liu, Y. Zhang, Z. Tu, X. Yang, F. Yang, Z. Wen, L. Zhu, R. Liu, Y. Li and L. Cui, *J. Mater. Chem. A*, 2015, **3**, 2794-2801.
39. H.-R. Kim, K.-I. Choi, K.-M. Kim, I.-D. Kim, G. Cao and J.-H. Lee, *Chem. Commun.*, 2010, **46**, 5061-5063.
40. C. W. Na, H.-S. Woo, I.-D. Kim and J.-H. Lee, *Chem. Commun.*, 2011, **47**, 5148-5150.
41. C. W. Na, H.-S. Woo and J.-H. Lee, *RSC Advances*, 2012, **2**, 414-417.
42. Y. Q. Liang, Z. D. Cui, S. L. Zhu, Z. Y. Li, X. J. Yang, Y. J. Chen and J. M. Ma, *Nanoscale*, 2013, **5**, 10916-10926.

TOC text

Three-dimensional untraporous network of NiO-ZnO is constructed for the detection of volatile organic compounds at room temperature under solar irradiation. The formation of p-n nanoheterojunctions not only increase the sensor response, but also improve the lower limit of detection, which provides guideline for the design of low-power solid-state chemical sensors in the near future.